RESEARCH ARTICLE

Editor's Choice

ADVANCED
OPTICAL
MATERIALS
www.advopticalmat.de

Tunable Ultra-Narrow Linewidth Light Source Through Liquid Crystal-Assisted Mini-Bound-States-In-Continuum Cavities

Renjie Tang, Yiting Wang, Jialing Jian, Zezhao Ju, Yalan Si, Jianghong Wu, Yuting Ye, Yilin Shi, Kangjian Bao, Yingchun Wu, Yiheng Tang, Chunlei Sun, Dawei Gao, Hongtao Lin, and Lan Li*

The introduction of liquid crystals into microcavities has garnered considerable attention for their exceptional tunability and high sensitivity to external perturbation factors within their distinct phase states. Here, a novel light source with both wavelength tunability and an exceptionally narrow linewidth is presented. This innovation is realized by strategically manipulating LC molecules, transitioning them from a well-aligned state to a disordered state with increasing temperature. The microcavity is tailored to support bound states in the continuum, a cutting-edge concept in photonic research that allows for light localization with minimal loss. In the pursuit of potential biocompatibility and to reduce cytotoxicity, indium phosphide colloid quantum dots are opted to serve as the emissive carriers within the system. An ultra-narrow linewidth light emission of 0.039 nm is observed, corresponding to a quality factor reaching 16668, along with a tunable range of 1.21 nm and a temperature sensitivity of 33.52 pm K^{-1}. The invention's compact size and tunable character make it an ideal candidate for a variety of potential applications, such as eco-friendly sensors with minimal ecological impact, optical modulators with precise control over light, and adaptable photonic devices that can be integrated with a diverse array of materials and configurations.

1. Introduction

Optical microcavities, characterized by their high-quality factors (Q-factor) and small mode volumes (V), are instrumental in driving progress in various scientific fields, such as nonlinear optics,[1–3] quantum electrodynamics (QED),[4–6] and the enhancement of photonic devices including filters,[7–9] sensors,[7,9,10] light sources[11–13] and spectrometers.[14–16] To improve the performance and broaden the functional range of optical microcavities, researchers are exploring the integration of novel materials with exceptional properties. Graphene, for instance, with its small insertion loss and high thermal conductivity, has been instrumental in the progression of microcavity-based electro-optic modulators,[17] photodetectors,[18] and lasers that either efficiently dissipate heat[19] or display improved emission performance.[20] Moreover, monolayer transition metal dichalcogenides (TMDs),

R. Tang
Zhejiang University
Hangzhou 310027, China

R. Tang, Y. Wang, J. Jian, J. Wu, Y. Ye, Y. Shi, K. Bao, Y. Wu, Y. Tang, C. Sun, L. Li
Key Laboratory of 3D Micro/Nano Fabrication and Characterization of Zhejiang Province
School of Engineering
Westlake University
Hangzhou 310030, China
E-mail: lilan@westlake.edu.cn

R. Tang, Y. Wang, J. Jian, J. Wu, Y. Ye, Y. Shi, K. Bao, Y. Wu, Y. Tang, C. Sun, L. Li
Institute of Advanced Technology
Westlake Institute for Advanced Study
Hangzhou 310024, China

Z. Ju, Y. Si, H. Lin
State Key Laboratory of Brain-Machine Intelligence
College of Information Science and Electronic Engineering
Zhejiang University
Hangzhou 310027, China

D. Gao
School of Micro-Nano Electronics
Zhejiang University
Hangzhou 310027, China

D. Gao
Zhejiang ICsprout Semiconductor Co. Ltd
Hangzhou 310000, China

L. Li
Westlake Institute for Optoelectronics
Fuyang, Hangzhou 311421, China

**ADVANCED
SCIENCE NEWS**

www.advancedsciencenews.com

**ADVANCED
OPTICAL
MATERIALS**

www.advopticalmat.de

renowned for their minuscule size gain media with potent excitonic emissions, contribute to the development of energy-efficient nanolasers.[13] Similarly, colloid quantum dots (cQDs) and perovskites, with their inherent amplification properties, have stimulated the creation of compact all-optical switching,[21] light-emitting diodes,[22,23] and nanolasers.[11,21,24,25]

Liquid crystals (LCs) have been recognized for their pronounced birefringence and capability to induce significant refractive index variation. Their long-range molecular order paired with fluid-like characteristics, endows them with distinctive properties not found in other materials. The integration of LCs into optical microcavities is a promising innovation,[26–28] with the remarkable tunability of LCs unlocking a wide array of practical applications, especially LC-microcavity-based light sources in light field modulation,[29] spectral wavelength tuning[27] and polarization control.[30] Additionally, the responsive character of LC-microcavity-based light sources makes them exceptionally well-suited for high-performance sensing of environmental factors such as temperature[27] and humidity,[31] as well as the detection of biomolecules[32] and ions.[33] However, despite these advancements, there are challenges to be addressed, such as the excessive spatial footprint of the devices, the clutter or disappearance of multiple longitudinal resonant modes during the tuning process, and the excessively sensitive detection that can lead to imprecise wavelength control in reverse.[28] Moreover, concerns arise with the use of certain luminescent materials, such as toxic CdSe cQDs, which may significantly restrict the potential for biosensing applications. A concerted effort to resolve these issues will further enable the integration of optical microcavities into a broader range of practical and environmentally safe applications. Bound states in the continuum (BIC) show great potential in resolving the issues mentioned previously. They have demonstrated efficacy in capturing light from the propagating wave continuum in free space and confining it within optical nanostructures, characterized by not only high Q-factors but also the ability to flexibly control the resonance wavelengths and modes via design manipulation. In addition, they exhibit topological vortex configurations in momentum space.[34] An abundance of novel discoveries have been made regarding BIC and their role in light-matter and light's spin-orbit interactions, and their practical applications have been extensively explored in areas such as harmonic generation,[35] lasing,[36–38] and sensing[39] applications.

In this research, we present a tunable light source with an ultra-narrow linewidth, utilizing the unique properties of LCs infused with eco-friendly indium phosphide (InP) cQDs. The resonator is constructed on a silicon nitride (SiN) substrate supporting a single-mode BIC mode, with a measured Q-factor of ≈8500. Subsequently, a blend of InP cQDs and photoresist was spin-coated onto an array of resonant cavities, resulting in an ultra-narrow linewidth light source with a remarkable value of 0.039 nm (Q-factor of 16 668) as well as a various of emission wavelengths within the cQDs' inherently broad fluorescence spectrum. Moreover, with the assistance of LCs, a specific resonant cavity within the array achieved a tuning range of 1.21 nm, alongside an average temperature sensitivity of 33.52 pm K^{-1}. This lower sensitivity indicates a superior precision in adjusting the wavelength of our light source by modifying the temperature. The capacity to precisely control the emission properties of our light source, without sacrificing its ultra-narrow linewidth,

paves the way for applications in precision spectroscopy, high-resolution imaging, and potentially quantum computing.

2. Results and Discussion

2.1. Cavity Design, Fabrication and Characterization

The schematic of a miniaturized BIC photonic crystal (PhC) cavity is depicted in **Figure 1a**. SiN is selected to demonstrate the concept due to its transparency in both the visible and near-infrared regions (Figure S1, Supporting Information). The PhC is created using a hexagonal lattice of air holes with a period (Λ) from 396 to 416 nm with a full-etching depth of 200 nm. Each cavity is composed of three regions with the same Λ, where the radius of the hole in the core region (r_a) is slightly larger than that (r_c) in the cladding region. A linear gradient change region is set in the middle, which can be expressed as follows:

$$r_{bi} = r_a - \frac{(r_a - r_c) * i}{N_b}, \; i = 1, 2, \ldots N_b \tag{1}$$

where i = 1 corresponds to the holes with the position closest to the core region. The transitional region serves the purpose of preventing the mutation of the effective refractive index, thereby minimizing scattering losses. The photonic band diagrams for transverse electric (TE) modes within the cladding region with infinite size are derived using the plane-wave expansion (PWE) method,[40] as illustrated in **Figure 2a**. Contrary to most defective PhCs that operate within a complete bandgap, our PhC functions above the light cone in the radiation continuum. Within this domain, BICs emerge at specific points where they do not couple to free space, yielding a theoretically infinite Q-factor. A prototypical BIC, known as a symmetry-protected BIC, resides at the Γ-point atop the second band (identified by a red dot). Enlarging the hole radius in the core region causes an upward frequency shift of the optical band while preserving the integrity of the Γ-point BIC mode. In our diagrams, only the BIC positions in the cladding are denoted (small black dot) for clarity, positioned within the incomplete bandgap of the cladding photonic crystal (orange region). The coupling between the core and higher-order cladding modes, which share the same frequency, is expected to be negligible due to mismatched effective indices and mode patterns. This disparity allows for a substantial reduction in the core area, even when the BIC becomes a quasi-BIC, while still retaining a high Q-factor owing to the robust lateral confinement provided by the cladding. The in-plane intensity distribution of the BIC mode, confined well within the core region, is displayed in inset i) of Figure 2a. Inset ii) presents finite-difference time-domain (FDTD) simulations revealing a sharp decline in the Q-factor from its peak (≈40 000) when the wave vector deviates slightly from the Γ-point, confirming the preservation of the BIC's standard mode. Our design eliminates the need for defect introduction and exhibits reduced sensitivity to symmetry perturbations,[11] ensuring stable Q-factors for exploring complex light-matter interactions.

Achieving high Q-factors in defective photonic crystals, such as L3 cavities, typically requires precise adjustment of the surrounding small hole positions.[41,42] However, difficulties arise when integrating these cavities with other materials, such as quantum
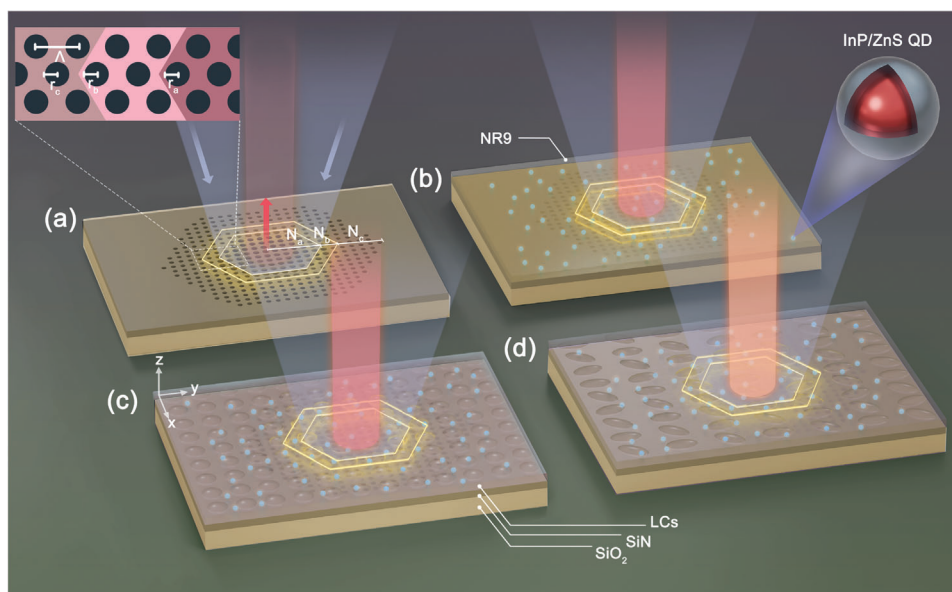
Figure 1. The operational principle of the tunable ultra-narrow linewidth light source. a) Schematic of the miniaturized BIC-based cavity in air surroundings. The inset provides a magnified zoomed-in view of the separation between the core, transitional, and cladding regions in the PhC slab, with the period and radius of each hole marked as Λ, r_a, r_b and r_c ($r_a = 0.28\Lambda$, $r_c = 0.25\Lambda$). The number of layers of air holes in each region denoted as N_a, N_b, and N_c, respectively (20, 6, and 40 in practice). b–d) Cavities with different cladding layers: mixtures of InP cQDs with photoresist (NR9 1500PY) (b), aligned LCs (c), and disordered LCs (d). The PL spectra are excited by blue light (473 nm), while the BIC mode (red light) is surface-emitting along the Z-direction.

dots, as it becomes challenging to ensure uniform micro-level arrangements, resulting in significant fluctuations in Q-factors. In many designs, fluorescent materials are usually mixed with polymers such as poly (methyl methacrylate) (PMMA).[43,44] This serves two purposes: first, to achieve a significant refractive index contrast with the cavity materials, and second, to prevent direct contact between the fluorescent material and water oxygen, thereby enhancing the longevity of the device. In this case, the random dispersion of fluorescent materials within the polymer layer leads to a significant local refractive index change, which further reflects the superiority of our design.

Here, we mixed the eco-friendly InP cQDs with the LCs as the fluorescence layer, where the cavity modes are highly sensitive to the LC phase's molecular spatial order, which can be controlled by temperature, as shown in Figure 2b. In the well-aligned phase, the LC molecules' radial alignment shifts with increasing temperature, inducing a blue shift in the resonance wavelength due to the negative thermo-optic coefficient.[45,46] Simulation results of the LCs' n_e variation prior to phase transition yielded a resonant-wavelength shift exceeding 1.5 nm, as depicted in Figure 2c. It is worth mentioning that since the substrate below the SiN slab is silicon oxide (SiO$_2$, n = 1.456), a more symmetrical refractive index distribution along the Z-axis is achieved as the refractive indices of the upper and lower layers converge, which theoretically enhances the Q-factor. Our innovative design strategically positions a second resonator with its peak wavelength (λ_2) set at the sum of the first device's peak wavelength (λ_1) and its tuning range ($\Delta\lambda_r$), which means $\lambda_2 = \lambda_1 + \Delta\lambda_r$. This arrangement enables the formation of a resonator array with the capacity for emission at any selected wavelength throughout the complete fluorescence spectrum, as exemplified in Figure 2d.

Then we successfully fabricated the designed PhC cavities, as characterized in the scanning electron microscopy (SEM) images featured in **Figure 3**a. The holes' actual size and depth parameters are shown in the inset diagrams, indicating that our fabrication process aligns well with our design. The steepness of the etching is high, and there are no common inclination problems[25] (additional images of the cavities are shown in FigureS2, Supporting Information). SiN possesses a subtle intrinsic fluorescence which, when paired with a cavity of sufficiently high Q-factor and subjected to intense pump power, allows for the detection of fluorescence directly related to the cavity's Q-factor (Figure S3, Supporting Information). The passive resonance curve of the cavity, as depicted in Figure 3b, is accurately fitted with a Lorentzian profile, revealing a linewidth of 0.073 nm and corresponding to a Q-factor of $\approx$8500. Inset i) in Figure 3b displays the charge-coupled device (CCD) image captured at the focal spot, where all the light energy is concentrated within the core region of the cavity.

In the selection of fluorescent substances, cQDs are renowned for their bandgap tunability, solution processability, and large absorption coefficients. However, the most widely used is the toxic CdSe cQDs, whose potential non-toxic substitutes often fall short in terms of quantum yield and stability. Here, we obtained eco-friendly InP cQDs with high quantum yields and mixed them with polymers to enhance their fluorescence stability. The quantum yield of our InP cQDs is impressively high, reaching up to 81.23%, as demonstrated in Figure 3c. Both phosphorus and indium have low toxicity. Modifying their surfaces, such as adding a layer of non-toxic shell material like zinc sulfide (ZnS), can prevent direct contact between quantum dots and samples, as well as the release of harmful ions, further enhancing their
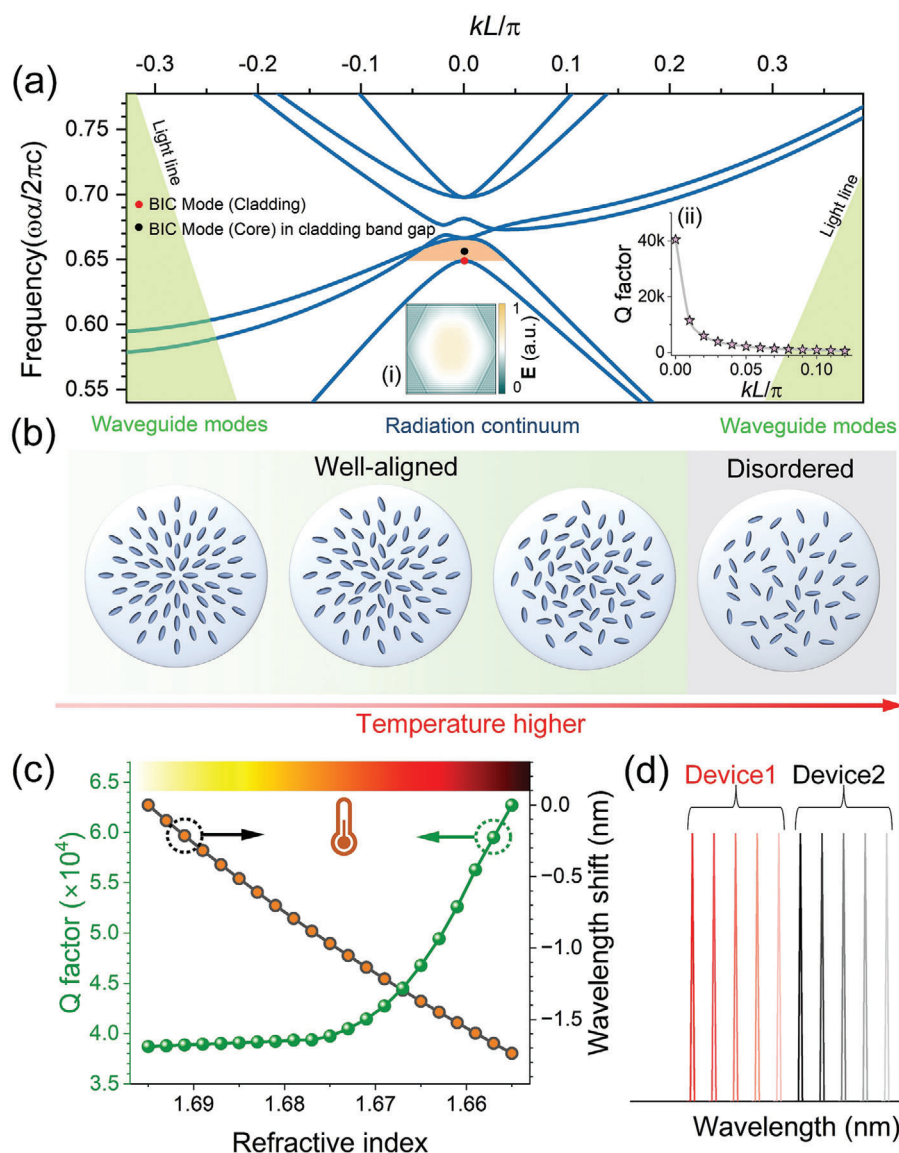
**ADVANCED
SCIENCE NEWS**

www.advancedsciencenews.com

**ADVANCED
OPTICAL
MATERIALS**

www.advopticalmat.de

Figure 2. a) Calculated photonic band structures with air holes of the cladding region (infinite size). The red and black dots represent the BIC modes in the cladding and core regions, respectively. The green area represents the area below the light cone while the orange area indicates the incomplete band gap formed by the cladding region near the Γ point. Inset i) is the in-plane intensity distribution of the black-dot BIC mode. Inset ii) is the simulated Q-factor of the black-dot BIC mode along the ΓX-direction wavevector (actual size). b) Spatial ordering of LC molecules from well-aligned to disordered phases. c) Relationship between cavity resonance Q-factor values and wavelength shifts with the refractive index of LCs. The horizontal coordinate covers the range of n_e change[47] of the LCs before phase transition as the temperature rises. d) Schematic diagram of the principle of arbitrary wavelength tuning in the cavity array.

biocompatibility and stability.[24,48] Transmission electron microscopy (TEM) provided evidence of the epitaxial growth of core-shell structures, as depicted in Figure 3d. Despite a notable lattice mismatch of ≈7% between the core and shell materials, the TEM images revealed distinct and unbroken lattice fringes across the entire quantum dot. This observation confirms the epitaxial relationship of the ZnS shell as it forms over the InP core. Further validation of these findings came from high-angle annular dark field scanning TEM (HAADF STEM) analysis, illustrated in Figure S4 (Supporting Information). The HAADF STEM images corroborated the presence of distinct lattice

fringes, reaffirming their size consistency with those observed in the conventional TEM representations.

2.2. Ultra-Narrow Linewidth Light Source

To rigorously evaluate the characteristics of our ultra-narrow linewidth light source, a homogeneous mixture of the photoresist NR9 1500PY with InP cQDs was evenly spin-coated atop the SiN slab. The chosen photoresist is exceptional for its optical transparency in the visible spectrum. Its chemical compatibility with
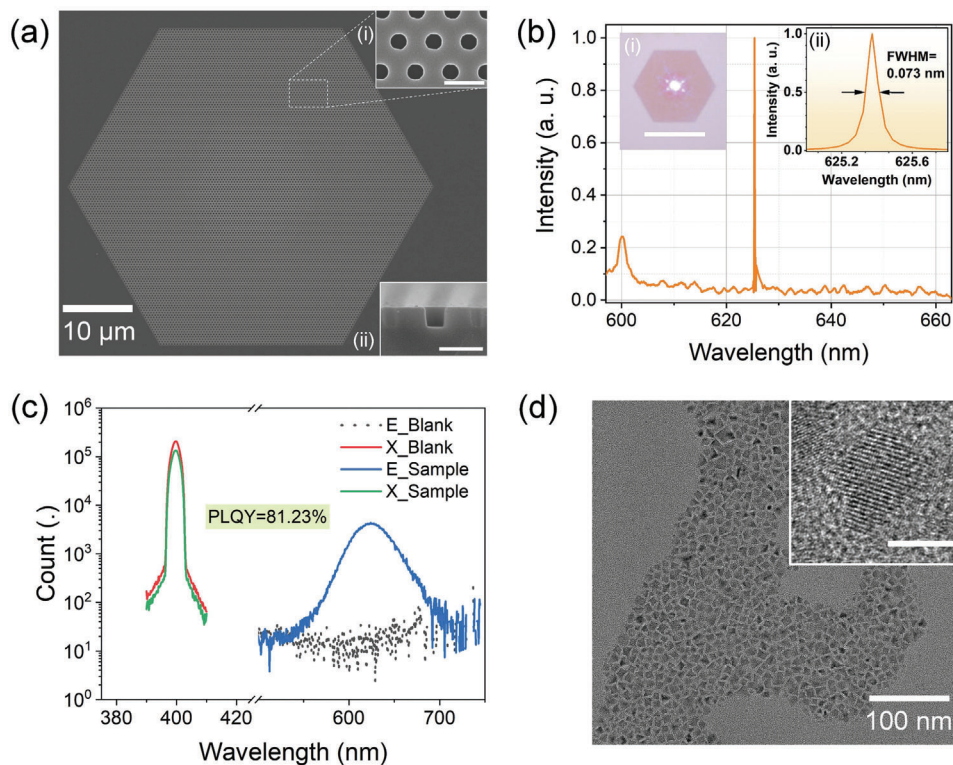
Figure 3. a) SEM images of the fabricated BIC-based PhC microcavity. Inset i) is the zoom-in view of the air holes in the cladding region. The scale represents 500 nm. Inset ii) is the longitudinal section view of the holes in the cladding region. The scale represents 400 nm. b) Measured photoluminescence (PL) spectrum of a fabricated sample with a Λ equal to 420 nm. Inset i) is the CCD image of the 473-nm laser spot focused on the cavity. Inset ii) is the Lorentzian fitting of the BIC mode showing a full width at half maximum (FWHM) of 0.073 nm. c) Excitation and emission spectra to determine the photoluminescence quantum yield (PLQY) of InP cQDs in toluene solution. d) TEM and high-resolution TEM (inset) images of the InP cQDs.

acetone facilitates the recyclability of the underlying cavity structure. This feature is particularly advantageous for sustainable research practices. A key attribute of NR9 1500PY is its refractive index, which is closely matched to that of SiO_2. This similarity ensures an optimal symmetric distribution of the refractive index along the Z-Z-direction of the device, as we previously discussed. It should be noted here that the effect of the cQDs on the refractive index of the photoresist is very small, and the relevant proof can be found in Figure S5 (Supporting Information).

In our experimental analysis, we employed a 473-nm laser as the excitation source, generating a pseudo-color mapping of the PL spectra dependent on varying pump powers for a PhC cavity with a Λ of 416 nm, as illustrated in **Figure 4a**. This visualization highlights the dynamic response of the cavity under different excitation conditions. We then directly compare the PL spectra from InP cQDs both within and outside the PhC cavity, specifically at a controlled pump power of 0.3 mW, as depicted in Figure 4b. The introduction of the PhC cavity induces a notable enhancement in PL intensity, reaching a peak value increase by a factor of 8.7 under this pump power. Figure 4c showcases the PL intensity variation as a function of the exciton pumping power for the cQDs situated in and out of the PhC cavity. With the pump intensity increasing, both the resonant peak and PL intensity show a linear increase, and then the resonant peak deviates from this behavior at a higher pump power of over 1 mW. The rate of increase in the resonant peak intensity has significantly

slowed while the PL intensity remains stable. This is likely related to the absorption saturation of cQDs, a phenomenon commonly reported in laser-related papers.[49–52] We further scrutinized the polarization characteristics of the emitted light by rotating a polarizer across different angles (inset in Figure 4c). The observed reduction in the resonance peak value along the Y-axis confirms the presence of linearly polarized components within that direction. The fluorescence polarization of the cQDs is isotropic, so the anisotropy results from the interaction with the BIC-based cavity. This transition represents an increase in the emission of photons with the same polarization, resulting in improved coherence, which signifies that our light source exhibits some laser-like properties. Upon increasing the pump power, we detected a modest blue shift in the resonance peak wavelength accompanied by a slight reduction in the Q-factor, attributable to thermally induced effects, as evidenced in Figure 4d. The decrease in Q-factor can be attributed to the thermal effect generated by the pumping spot, leading to a change in the local refractive index, and an increase in scattering loss. Our comprehensive spectral analysis across the entire fluorescence range yielded exceptionally sharp resonant peak spectra from the period-variable cavity array (Figure 4e). We established a linear relationship between the resonant wavelength and the periodicity of the PhC lattice, with a slope of 1.336. Notably, the Q-factor of our light sources consistently exceeded 10 000, with an impressive peak value of 16 668 (Figure 4f). Leveraging these findings, we can infer that a
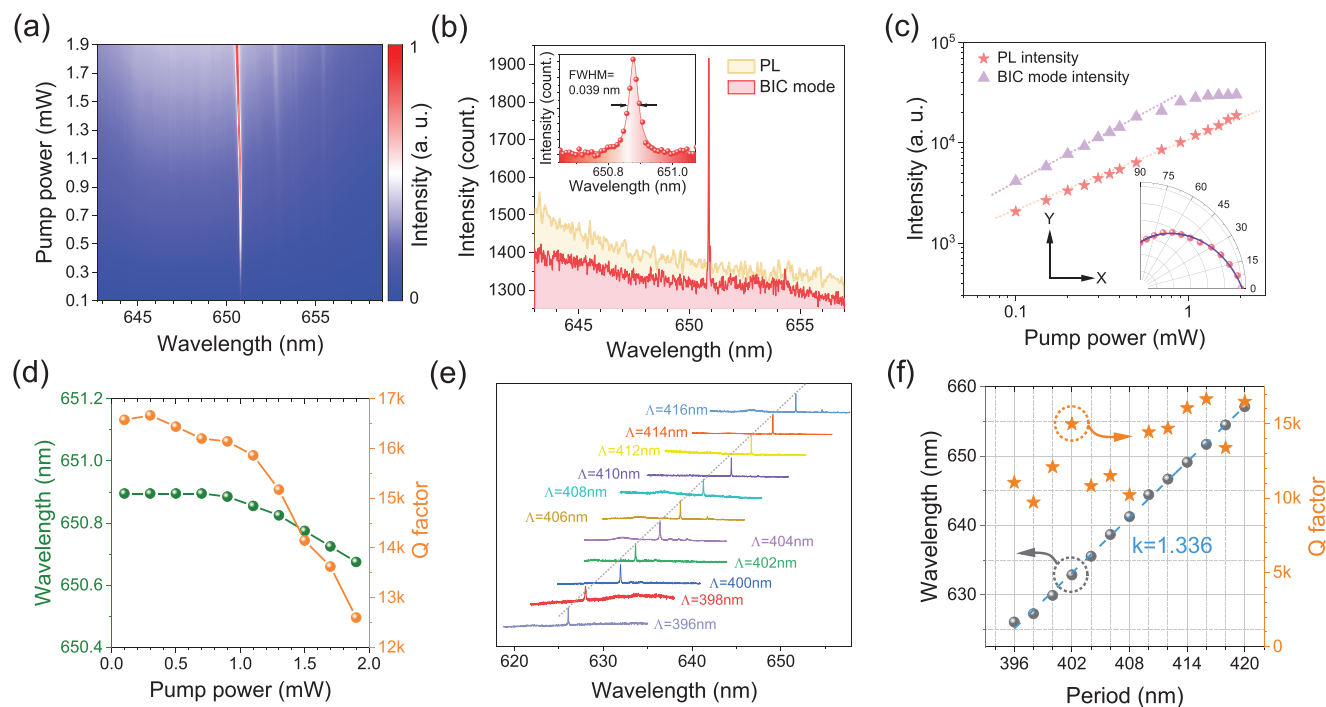
ADVANCED
SCIENCE NEWS

www.advancedsciencenews.com

ADVANCED
OPTICAL
MATERIALS

www.advopticalmat.de

Figure 4. a) 2D pseudo-color mapping of pump power-dependent PL spectra for the cavity (Λ = 416 nm). b) Comparative analysis of the PL spectra for InP cQDs in (red) and out of (light brown) the BIC-based cavity at a pump power of 0.3 mW. Inset is the Lorentzian fitting of the peak indicating an FWHM of 0.039 nm. The red dots are the actual data points, indicating that the resolution of the spectrometer is adequate. c) Relationship between PL intensities and excitation power for the cQDs on a double-logarithmic scale, distinguishing those situated within the BIC-based cavity (purple curve) from those outside (red curve). The inset details the polarization properties of the PL emission from the InP cQDs in the BIC cavity. d) The center wavelength and Q-factor of the resonant peak at different pump powers. e) PL spectra of cavities with different periods from 396 to 416 nm. The black dashed line indicates the trace of the peak position. f) Center wavelengths of the resonant peak for cavities with different periods fitted with a slope of 1.336. On the right Y-axis, the corresponding Q-factors are displayed.

mere 0.75 nm adjustment in the lattice period is required to shift the resonant peak wavelength by 1 nm. Such precision is readily achievable with our electron beam lithography (EBL) process, thanks to our electron beam's tight focusing capability, typically maintained within a 40 nm diameter with a minimum moving step of 0.1 nm. This level of control underscores the robustness and versatility of our fabrication technique, paving the way for finely tuned photonic devices.

2.3. Liquid Crystal-Assisted Tunability

To advance our photonic device research, we mixed the cQDs with LCs until they reached a uniform dispersion state, then spin-coated them onto a series of cavities for an even distribution after the film formed. For precise thermal control, we placed the samples within a carefully sealed heating enclosure, allowing us to calibrate the temperature accurately, an essential aspect of investigating temperature-dependent optical phenomena. The sample was capped with an adiabatic quartz sheet, selected for its thermal insulative properties to minimize heat loss and ensure that it does not interfere with our optical measurements. Using the same analytical techniques as previously applied, we conducted tests at ambient temperature, observing resonant peak spectra akin to those acquired at our earlier tests. These spectra, captured and depicted in **Figure 5a**, exhibit a strong dependency on

the ambient temperature, a key variable in our study. Our observations revealed that the resonant wavelengths exhibit a discernible blue shift with a temperature rise. This shift becomes particularly pronounced near the liquid crystal phase-transition temperature, identified at 65.2 °C. By carefully adjusting the periodicity of the cavities, we successfully aligned the resonant wavelength of a second unheated device to closely approach the phase-transition point of the first heated device. This strategic approach allows us to selectively target any desired emission wavelength within the cQDs' fluorescence spectrum (Figure S6, Supporting Information) across our integrated on-chip array.

Figure 5b presents a detailed account of the resonant peak line widths across various temperatures. The data indicates some level of fluctuation; however, the general trend is a decrease in linewidth, corroborating our previous simulations. This is because the BIC mode in this design is fundamentally a symmetry-protected BIC. Therefore, as the refractive indices of the upper and lower cladding layers approach similarity, the symmetry is enhanced, subsequently leading to an increase in the Q-value. Figure 5c is a granular analysis of the resonant wavelength stability, which showcases the wavelength fluctuations at three distinct temperatures: 40, 50, and 60 °C. At these temperatures, the resonant wavelengths exhibit remarkable stability, with standard deviations of 24.5, 20.4, and 34.5 picometers, respectively, suggesting only minor variations in the noise floor. Furthermore, we delved into the temporal responsiveness of our thermal sensor
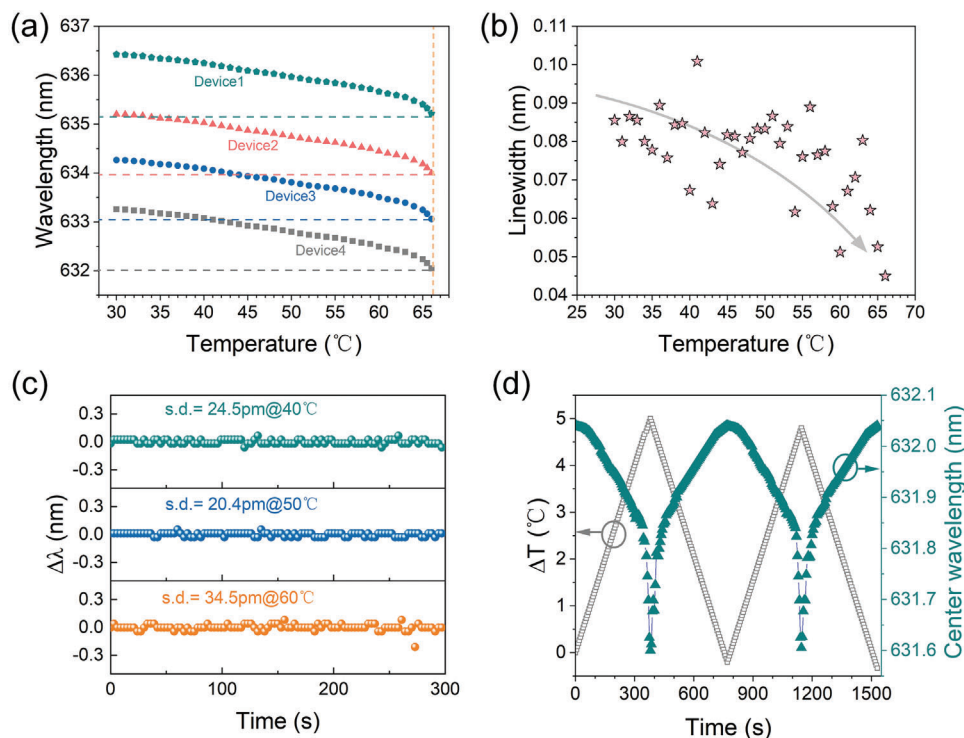
**ADVANCED
SCIENCE NEWS**

www.advancedsciencenews.com

**ADVANCED
OPTICAL
MATERIALS**

www.advopticalmat.de

Figure 5. a) Experimental resonant wavelengths of 4 different devices at different temperatures. b) Emission linewidth of the same device at different temperatures. The gray arrow marks the trend of line-width change. c) Resonant wavelength stability of the LC-cQDs microcavity at three distinct temperatures, showcasing the robustness of the system across different thermal conditions. The lasing wavelength variations are quantified and communicated via the indicated standard deviations (s.d.). d) The temporal behavior of the resonant wavelength is captured (represented by green dots) as the microcavity operates in proximity to its phase-transition threshold. Here, the resonant wavelength's reaction to real-time temperature changes (shown with gray dots) is monitored.

by subjecting it to repeated temperature alterations. The results, recorded in Figure 5d (represented by the gray curve), affirm that the resonance wavelength promptly and reliably mirrors the changes in environmental temperature, demonstrating excellent repeatability. Crucially, we note that the phase-transition temperature of the resonant wavelength can be custom-tailored by selecting different liquid crystal materials. This adaptability allows us to fine-tune our devices to meet the specific requirements of various applications, highlighting the versatility and potential for customization in our photonic device design.

3. Discussion

Table S1 (Supporting Information) presents a comprehensive overview of the fine-tuning ultra-narrow linewidth light source with liquid crystal assistance. The field of tunable light sources utilizing LCs is burgeoning, with prevalent configurations involving dyes incorporated into various LCs' self-assembly microcavity structures such as microspheres,[26,27,33] distributed feedback (DFB) lasers,[53] and distributed Bragg reflector (DBR) lasers.[54] These systems are lauded for their expansive tuning capabilities, driven by their acute sensitivity to temperature variations. However, this thermal sensitivity, while advantageous for broad-range tuning, can pose significant challenges when a fixed wavelength output is required.[28] The propensity for substantial wavelength drift in response to minute temperature fluctuations makes

achieving and maintaining a precise wavelength a complex task. To mitigate these effects, one might consider employing liquid crystals with a less pronounced temperature dependency on their pitch length, integrating polymerizable cholesteric liquid crystals (CLCs), or implementing exceptionally accurate temperature control mechanisms.[28] Yet, these solutions come with a trade-off—increased complexity and cost—which can hinder the practical deployment of such devices.

For applications where temperature sensitivity is not desirable, such as non-temperature-sensitive sensing, excessive responsiveness to temperature can be more of a hindrance than a help, complicating the control of the system. In our work, we have tailored our approach to harness the higher refractive index of the silicon nitride layer, which confines the light's mode field more efficiently. Consequently, the resonant peak wavelength can be finely adjusted via the refractive index of the LCs, significantly alleviating the stringent requirements for temperature control and enhancing the precision of such adjustments. Our device not only exhibits superior Q-factors when compared to those reported in existing literature but also demonstrates a marked reduction in temperature sensitivity. This crucial advancement underscores our success in achieving high-precision control, a notable design strength. Although the tunability range may be perceived as limited, this is effectively offset by the deployment of an array of high-precision cavities (expanded to 25.7 nm), facilitating a broad spectrum of selectable wavelengths.

**ADVANCED
SCIENCE NEWS**

www.advancedsciencenews.com

**ADVANCED
OPTICAL
MATERIALS**

www.advopticalmat.de

From a materials perspective, the environmentally benign InP cQDs are a noteworthy component. First reported for laser emission in 2011, InP has not seen substantial advancements in emission properties, particularly in achieving narrow linewidths—until now. While we have yet to conclusively demonstrate that our ultra-narrow linewidth light source constitutes a laser, which would necessitate a battery of rigorous tests including coherence,[55] second-order coherence for the thermal state,[12,56,57] and amplified spontaneous emission (ASE)[23] analyses, the current emission characteristics could be interpreted as a "cold cavity" resonance.[13] Should future developments enable us to achieve lasing, this would signify a landmark breakthrough, denoting an even narrower linewidth and solidifying a new frontier in laser technology.

4. Conclusion

In conclusion, we have successfully engineered a liquid crystal-assisted, finely tunable ultra-narrow linewidth light source. Our innovative approach has led to the realization of remarkably narrow linewidth emissions (0.039 nm), showcasing an exceptionally high Q-factor of 16668. This peak performance spans the entire fluorescence peak range, offering tremendous versatility. Our device demonstrates a substantial tuning capability of 1.21 nm, combined with an impressive temperature sensitivity of 33.52 pm K^{-1}. This level of temperature sensitivity is of paramount importance for precision-tuned light sources, providing fine control over the emission wavelength in response to minute changes in temperature. One of the pivotal aspects of our design is the utilization of quantum dots, which affords us the flexibility to extend the operational wavelength range. By capitalizing on this feature, we can adapt our light source to cover broader spectral domains, including the longer wavelengths of visible light and even extending into the near-infrared region.[25,49–51] The results reveal the opportunities in precision spectroscopy, high-resolution imaging, and potentially even quantum computing. Furthermore, our use of non-toxic materials underscores the potential for this technology to be safely applied in biological contexts. This characteristic, combined with the light source's sensitivity and tunability, makes it an invaluable tool for applications in non-toxic detection and biological sensing.

5. Experimental Section

Experimental details, including PhC cavity fabrication, film fabrication and deposition, and optical characterization, are listed in the Experimental section in Supporting Information.

Supporting Information

Supporting Information is available from the Wiley Online Library or from the author.

Acknowledgements

Conflict of Interest

The authors declare no conflict of interest.

Data Availability Statement

The data that support the findings of this study are available from the corresponding author upon reasonable request.

Keywords

[1] X. Zhang, Q.-T. Cao, Z. Wang, Y.-x. Liu, C.-W. Qiu, L. Yang, Q. Gong, Y.-F. Xiao, *Nat. Photonics* **2019**, *13*, 21.

[2] J.-h. Chen, X. Shen, S.-J. Tang, Q.-T. Cao, Q. Gong, Y.-F. Xiao, *Phys. Rev. Lett.* **2019**, *123*, 173902.

[3] T. Kippenberg, S. Spillane, K. Vahala, *Phys. Rev. Lett.* **2004**, *93*, 083904.

[4] S. Spillane, T. Kippenberg, K. Vahala, K. Goh, E. Wilcut, H. Kimble, *Phys. Rev. A* **2005**, *71*, 013817.

[5] J. Vučković, Y. Yamamoto, *Appl. Phys. Lett.* **2003**, *82*, 2374.

[6] J. Vučković, M. Pelton, A. Scherer, Y. Yamamoto, *Phys. Rev. A* **2002**, *66*, 023808.

[7] R. Tang, C. Sun, K. Bao, Z. Chen, Z. Ju, M. Wei, Y. Wu, J. Wu, K. Xu, H. Lin, L. Li, *Laser Photonics Rev.* **2023**.

[8] C. Sun, Y. Yin, Z. Chen, Y. Ye, Y. Luo, H. Ma, L. Wang, M. Wei, J. Jian, R. Tang, *PhotoniX* **2022**, *3*, 12.

[9] H. Yan, Y. Zou, S. Chakravarty, C.- J. Yang, Z. Wang, N. Tang, D. Fan, R. T. Chen, *Appl. Phys. Lett.* **2015**, *106*, 121103.

[10] T. Yoshie, L. Tang, S.-Y. Su, O. Microcavity, *Sensors* **2011**, *11*, 1972.

[11] R. Tang, Y. Shi, H. Shang, J. Wu, H. Ma, M. Wei, Y. Luo, Z. Chen, Y. Ye, J. Jian, X. Zheng, H. Lin, L. Li, *Nanophotonics* **2023**, *12*, 3257.

[12] Y. Ren, P. Li, Z. Liu, Z. Chen, Y.-L. Chen, C. Peng, J. Liu, *Sci. Adv.* **2022**, *8*, eade8817.

[13] Y. Li, J. Zhang, D. Huang, H. Sun, F. Fan, J. Feng, Z. Wang, C. Z. Ning, *Nat. Nanotechnol.* **2017**, *12*, 987.

[14] C. Sun, Z. Chen, Y. Ye, K. Lei, H. Ma, M. Wei, R. Tang, J. Wu, H. Lin, L. Li, *Laser Photonics Rev.* **2023**, *17*, 2200792.

[15] C. Sun, Z. Chen, Y. Yin, Y. Ye, Y. Luo, H. Ma, J. Jian, Y. Shi, C. Zhong, D. Zhang, *ACS Photonics* **2022**, *9*, 2973.